J Electroceram (2007) 18:219–224
DOI 10.1007/s10832-007-9027-4

Electrical conductivity of $Nd_{1-x}Ca_xSc_{1-y}Mg_yO_3$ perovskite-type oxides

Hisashi Kato · Hiroo Yugami

Received: 19 July 2006 / Accepted: 23 December 2006 / Published online: 23 February 2007

Abstract The electrical conductivities of $Nd_{1-x}Ca_xSc_{1-y}Mg_yO_3$ were measured in the temperature range from 673 to 1273 K under both wet and dry conditions. The optimum Ca^{2+} doping concentration to the Nd^{3+} site in $NdScO_3$ was found to be the range from 5 to 10%. Hole conduction was predominant under dry and highly oxidized conditions of $P(O_2)>10^{-2}$ kPa in the temperature range from 973 to 1273 K, and proton conduction was predominant under wet and reduced conditions in the temperature range from 673 to 973 K. Oxide ion conduction was predominant under wet and reduced conditions in the temperature range from 1073 to 1273 K. The Mg^{2+} doping concentration limit for the Sc^{3+} site to hold a single crystal phase was 2%, and this doping enhanced hole conduction.

Keywords Electrical conductivity · Perovskite · Scandium oxide · Proton conduction

1 Introduction

Solid oxide fuel cells (SOFCs) are expected to act as high-efficiency power generating systems [1, 2]. However, there are problems associated with these fuel cells, such as cost and long-term stability, because they necessarily operate at temperatures as high as 1273 K [3]. In order to solve these problems, the development of SOFCs that operate in the temperature range from 873 to 1073 K is currently underway [4]. With regard to the electrolyte material, a number of efforts are being made to reduce the operating temperature. One such effort involves research and development concerning thin film solid electrolytes, for example YSZ, which are used as an electrolyte material in high temperature SOFCs [5]; another concerns the research and development of material with high ionic conductivity at moderate temperatures [6]. The perovskite-type oxides based on $LaGaO_3$ have been intensively studied throughout the world as materials with high ionic conductivity [7–9]. These materials were initially identified by Ishihara et al. and show very efficient conduction characteristics such as 0.35 S/cm at 1223 K for doped $LaGaO_3$ [8].

Kilner and Brook found that migration enthalpy ΔH_m decreases with increasing critical radius r_{crit} calculated from the A_2B triangle of the ABO_3 structure with respect to the ionic conductivity of perovskite-type oxides [10]. Cook and Sammells report the relationships among free volume, FV, average metal-oxygen bond energy, E_{ab}, r_{crit}, Tolerance Factor, t, and electrical conductivity [11], noting that as FV, r_{crit} and E_{ab} increase, ΔH_m decreases. Additionally, Hayashi et al. reviewed the relationship between structure and conductivity in perovskite-type oxides, finding optimum combinations between host and dopant ions; specifically, the optimum dopant for La^{3+} in the A site is Sr^{2+} and that for Nd^{3+} is Ca^{2+} [12]. They also report that the maximum point exists near 0.96 on t, and that the mobility of the oxide ion is improved as FV increases. Since large FV and r_{crit} are expected in perovskite-type oxides which contain scandium or indium for the B-site ion, which has larger ionic radii than gallium, the high ionic mobility is also expected.

H. Kato (✉)
Tohoku Electric Power Co., Inc.,
7-2-1, Nakayama, Aoba-ward,
Sendai 981-0952, Japan
e-mail: h-kato@rdc-tohoku.jp

H. Yugami
Graduate School of Engineering, Tohoku University,
Aoba 01, Aramaki, Aoba-ward,
Sendai 980-8579, Japan

With this background, research on conduction characteristics has been carried out [13–19]. Nomura and Tanase examined the conduction characteristics of perovskite-type oxides including $La_{0.9}Sr_{0.1}M^{III}O_3$ (M^{III}=Al,Ga,Sc,In and Lu), reporting that $La_{0.9}Sr_{0.1}GaO_3$ was the most efficient conductive material from the viewpoint of crystallographic symmetry [13]. They also state that the conductivity of $La_{0.9}Sr_{0.1}ScO_3$ was low because its relative density has not yet been sufficiently improved.

It has been reported by Kim et al. [15], Nomura et al. [16, 17] and Lybye and Bonanos [18] that $LaScO_3$-based materials show high proton conductivity. Lybye and Bonanos report that in the temperature range of 1073 K or less under low oxygen partial pressure, proton conduction becomes dominant in $La_{0.9}Sr_{0.1}Sc_{0.9}Mg_{0.1}O_3$ [18]. Furthermore, Nomura et al. report that proton conduction is predominant in the temperature range of 873 K or less under low oxygen partial pressure in a wet hydrogen atmosphere [16]. $La_{0.8}Sr_{0.2}ScO_3$ shows a conductivity of 6×10^{-3} S/cm at 873 K [17]. In addition, Fujii et al. have also reported the proton conductivity of $Ln^{III}ScO_3$ (Ln^{III}= La,Nd,Sm,Gd), although they report the conduction characteristics only for $Nd_{0.9}Ca_{0.1}ScO_3$ in $Nd(Ca)ScO_3$ series [19]. However, little is yet known about the optimum doping concentration for the Nd^{3+} site and its detailed electrical properties.

In a previous study, we investigated the conduction characteristics of the $La(Sr)ScO_3$ oxides and found that $La_{0.675}Sr_{0.325}Sc_{0.99}Al_{0.01}O_3$ showed high oxygen ionic conductivity [20]. In the present study, we investigated the conduction characteristics and optimum doping concentration for the Nd^{3+} site in $Nd_{1-x}Ca_xScO_3$. We also report the effects on electrical conductivity of Mg^{2+} doping of the Sc^{3+} site.

2 Experimental procedures

2.1 Sample preparation and characterization

All samples were synthesized by the solid state reaction method. Reagent grade Nd_2O_3 (Koujyundo Chemicals, 99.9%), Sc_2O_3 (Soekawa Chemicals, 99.9%), $CaCO_3$ (Kanto Chemicals, 99%) and MgO (Kanto Chemicals, 99%) were used as starting materials. Stoichiometric amounts of these materials were mixed for 12 h in a ball mill and calcinations were carried out twice at 1673 K for 5 h. The calcined powder was reground and pressed into a pellet at 20 Mpa, and the pellet was then fired at 1873 K for 12 h. The identification of phases was carried out by powder X-ray diffraction (XRD) with Cu–Kα radiation using a Rigaku RINT-2500 diffract meter. The lattice constant was determined by the least squares method based on the diffraction peak. It was confirmed that the relative density of the sample was over 0.94. Quantitative analysis of the composition was performed by inductively coupled plasma (ICP) measurement, and the differences between nominal and actual composition were estimated to be from 5% short to 1% excess for Nd and 1% excerss for Ca as compared to the molar ratio of Sc.

2.2 Electrical conductivity measurement

Electrical conductivity was measured by the AC method in the temperature range from 673 to 1273 K. AC conductivity was obtained by impedance spectroscopy, using an impedance meter (Solartron 1260 FRA and PAR283 potentiostat) over a frequency range of 10 Hz-1 MHz. After shaping the sample pellet into a rectangular parallelepiped, a platinum electrode was installed on the double end, and the pellet was fired at 1273 K for 2 h. Electrical conductivities were measured under dry air, wet ($P(H_2O)$= 3.14 kPa) and controlled $P(O_2)$(10^{-20} kPa<$P(O_2)$<21 kPa) conditions.

3 Results and discussion

3.1 Optimum Ca^{2+} doping concentration for the Nd^{3+} site in $NdScO_3$

The XRD patterns of $NdScO_3$ oxides with several different dopant compositions are shown in Fig. 1. $Nd_{1-x}Ca_xScO_3$ was identified as an orthorhombic phase; $Nd_{0.95}Ca_{0.05}ScO_3$ and $Nd_{0.92}Ca_{0.08}ScO_3$ were identified as single phase. Other oxides over x=0.1 include impurities such as $CaSc_2O_4$, and unknown materials, as shown in Fig. 1. High-temperature XRD measurement identified these oxides with impurities as non-single phase from room temperature to 1273 K. Fujii et al. report that $Nd_{0.9}Ca_{0.1}ScO_3$

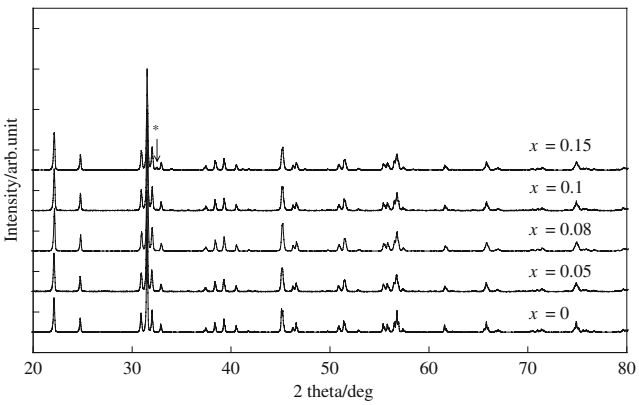

Fig. 1 X-ray diffraction patterns of $Nd_{1-x}Ca_xScO_3$ perovskite oxides. Three oxides (x=0, 0.05, 0.08) were identified as single phase, the others were identified as mixed phase. *Asterisk*: impurity phase $CaSc_2O_4$

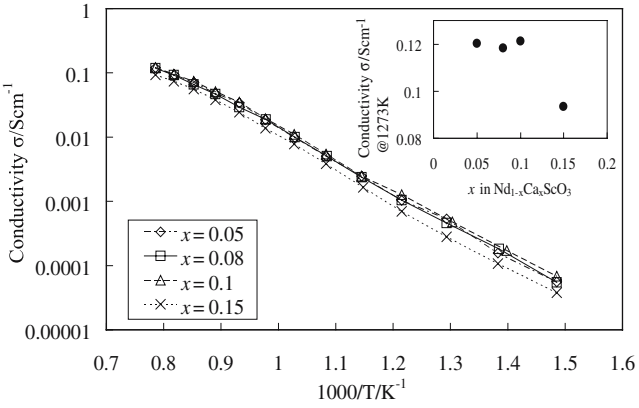

Fig. 2 Arrhenius plots of σ for $Nd_{1-x}Ca_xScO_3$ under wet air conditions

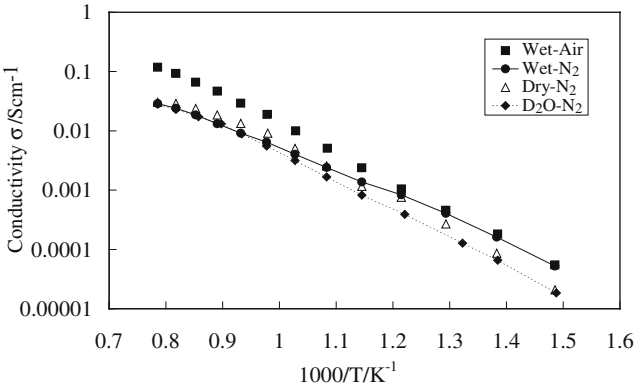

Fig. 3 Arrhenius plots of σ for $Nd_{0.92}Ca_{0.08}ScO_3$ under H_2O/air, dry N_2, H_2O/N_2 ($P(H_2O)$=3.14 kPa) and D_2O/N_2($P(D_2O)$=3.14 kPa) conditions between 673 and 1273 K

was identified as a single-phase oxide [19], however, the single phase of $Nd_{0.9}Ca_{0.1}ScO_3$ was not obtained in the present synthesis method.

Figure 2 shows the Arrhenius plots of single-phase oxides and $Nd_{0.9}Ca_{0.1}ScO_3$ under wet air conditions. In the range of x=0.05 to x=0.1, conductivity showed almost the same values, but it decreased in the range over x=0.1 at 1273 K. For x=0.1, an impurity phase was identified in the lattice. However, the present results suggest that the ionic and/or electronic conduction pass is not inhibited in the high-temperature range. For x=0.15, conductivity was decreased, suggesting that the impurity phase makes the inhibition of the conduction path. Consequently, the optimum doping concentrations were found to range from 5 to 10%.

3.2 Electrical conductivity of Nd(Ca)ScO_3

Figure 3 shows the Arrhenius plots of the conductivity of $Nd_{0.92}Ca_{0.08}ScO_3$ between 673 and 1273 K under dry and wet conditions. Below 873 K, σ_t, total electrical conductivity, under wet conditions showed a higher value than that under dry condition, and below 1023 K, an H^+/D^+ isotope effect was observed, suggesting the appearance of proton conduction under these conditions. Above 873 K, the σ_t values under wet N_2 conditions and dry N_2 conditions were higher than those under wet H_2 conditions. This suggests that hole conduction is predominant under these conditions.

Figure 4 shows the $P(O_2)$ dependence of σ for $Nd_{0.92}Ca_{0.08}ScO_3$ at 873, 1073 and 1273 K under dry and wet ($P(H_2O)$=3.14 kPa) conditions. The σ values fit the following equation:

$$\sigma_t = \sigma_{\text{ion}} + \sigma^0_{\text{hole}} P(O_2)^{1/4} \quad (1)$$

where σ_{ion} is the ionic conductivity and σ^0_{hole} is the hole conductivity at $P(O_2)$=1 atm. At 1273 K, σ_{ion} was 5.7×10^{-3} S/cm and σ^0_{hole} was 0.104 S/cm. At 873 K, σ_{ion} was 1.1×10^{-3} S/cm and σ^0_{hole} was 1.3×10^{-3} S/cm. σ^0_{hole} was decreasing dramatically with decreasing temperatures. At $P(O_2)>10^{-2}$ kPa, σ_t is dependent on $P(O_2)$, suggesting that hole conduction is predominant. On the other hand, σ_t is independent of $P(O_2)$ at $P(O_2)<10^{-8}$ kPa, suggesting that ionic conduction is predominant and the presence of n-type conduction was eliminated. In a comparison of dry and wet conditions, σ_t under dry conditions was higher than that under wet conditions under $P(O_2)>10^{-1}$ kPa at 1073 K and $P(O_2)>$ 1 kPa at 873 K.

In a dry oxygen atmosphere, the formation of electron holes is described by

$$\frac{1}{2}O_2(g) + V_{\ddot{O}} = O^x_O + 2h^{\cdot}. \quad (2)$$

In a wet oxygen atmosphere, both protons and electron holes are generated according to Eqs. 3 and 4:

$$H_2O(g) + V_{\ddot{O}} + O^x_O = 2OH_{\dot{O}} \quad (3)$$

and

$$H_2O(g) + 2h^{\cdot} + 2O^x_O = 2OH_{\dot{O}} + \frac{1}{2}O_2(g) \quad (4)$$

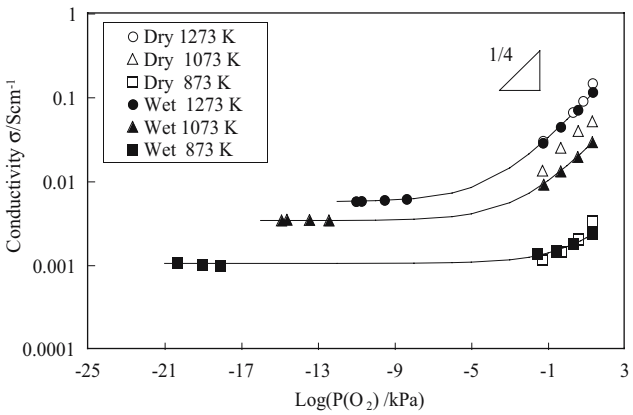

Fig. 4 Electrical conductivities as a function of oxygen partial pressure at 1273, 1073 and 873 K under dry and wet conditions ($P(H_2O)$= 3.14 kPa) for $Nd_{0.92}Ca_{0.08}ScO_3$

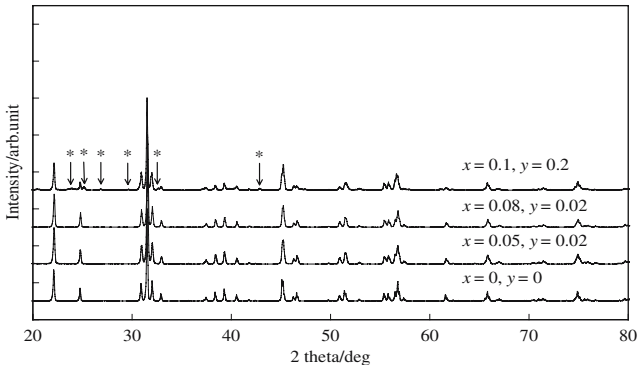

Fig. 5 X-ray diffraction patterns of $Nd_{1-x}Ca_xSc_{1-y}Mg_yO_3$. *Asterisk*: impurity phase such as $CaSc_2O_4$,Nd_2O_3,MgO and unidentified peaks

where $V_O^{\cdot\cdot}$, O_o^x, $h^{\cdot}$ and OH_O are oxygen vacancy, oxygen ion on the oxygen site, an electron hole and hydroxyl ion on the oxygen site, respectively.

With decreasing temperature, $P(H_2O)$ is increasing because the equilibrium shifts the formation of H_2O in Eq 5:

$$H_2O(g) = H_2(g) + \frac{1}{2}O_2(g) \tag{5}$$

Because of the formation of H_2O, equilibriums shift the formation of OH in Eqs. 3 and 4. This suggests that the dominant charge carrier changes from electron holes to protons with decreasing temperature under wet conditions.

At 1273 K, hole conduction is predominant under wet conditions. Therefore, the difference between dry and wet conditions was not observed. On the other hand, the electron holes decrease because the equilibrium shifts the formation of OH in Eq. 4 at 1073 K. Therefore, the proton conduction is expected to appear in a low concentration under wet conditions. However, the mobility of protons is expected to be smaller than that of holes. Consequently, it is expected that the difference between the conductivity under dry conditions and that under wet conditions appear at 1073 K as shown in Fig. 4.

$Nd(Ca)ScO_3$ was found to be the mixed conductor. Hole conduction is predominant in the high temperature and the high $P(O_2)$ range and proton conduction is predominant in the lower temperature range under wet conditions.

3.3 Effect of Mg^{2+} doping on the Sc^{3+} site in $Nd_{1-x}Ca_xScO_3$

In order to investigate the effect of Mg^{2+} doping on the electrical conductivity in $Nd(Ca)ScO_3$, we attempted to carry out Mg^{2+} doping on the Sc^{3+} site. Figure 5 shows the XRD patterns of $Nd_{1-x}Ca_xSc_{1-y}Mg_yO_3$. At doping concentrations of over 2% for the Sc^{3+} site, it was found that the impurity phase such as a starting material, MgO and $CaSc_2O_4$ appeared in the orthorhombic phase. Therefore, the solubility limit of Mg^{2+} for the Sc^{3+} site is 2% in Nd-(Ca)ScO_3. Arrhenius plots of the electrical conductivities under wet air conditions are shown in Fig. 6. Electrical conductivity not only improved under Mg^{2+} doping but also declined in $Nd_{0.95}Ca_{0.05}Sc_{0.98}Mg_{0.02}O_3$. Figure 7 shows the ionic transference number t_{ion} defined as below:

$$t_{ion} = \sigma(\text{wet}H_2)/\sigma(\text{dryair}) \tag{6}$$

where σ ($wetH_2$) is the conductivity under wet H_2 conditions and σ (dryair) is that under dry air conditions. A comparison between y=0 and y=0.02 in $Nd_{0.92}Ca_{0.08}Sc_{1-y}Mg_yO_3$ showed that t_{ion} decreases as $y$increases, as shown in Fig. 7. It was found that hole conduction improves under Mg^{2+} doping for the Sc^{3+} site. It is expected that these hole conduction results will have practical applications to SOFC cathode intermediate and hydrogen purification membrane.

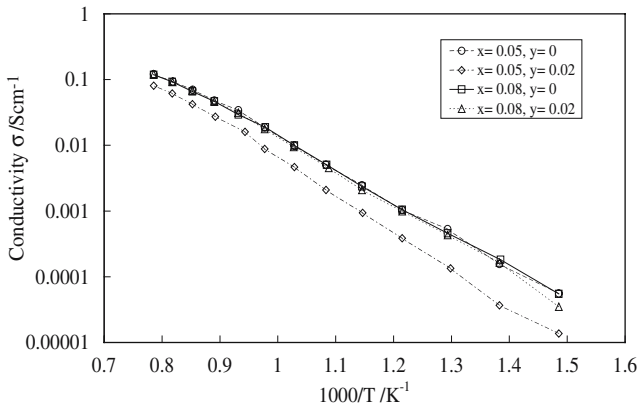

Fig. 6 Arrhenius plots of σ for $Nd_{1-x}Ca_xSc_{1-y}Mg_yO_3$ under wet air conditions

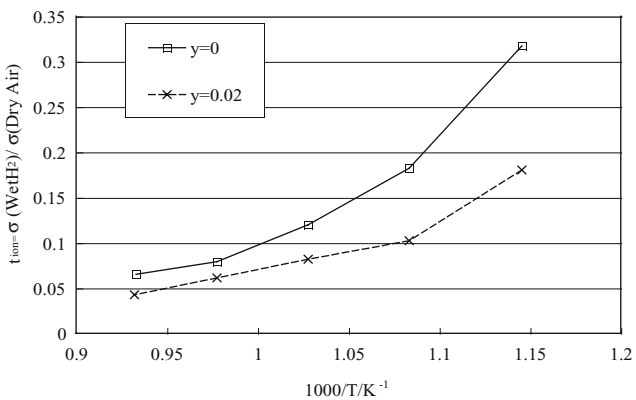

Fig. 7 Ionic transport number t_{ion} of $Nd_{0.92}Ca_{0.08}Sc_{1-y}Sc_yO_3$. t_{ion} is defined by the following equation: $t_{ion} = \sigma(\text{wet}H_2)/\sigma(\text{dry air})$

Table 1 Activation energy and electrical conductivity of $Nd_{1-x}Ca_xsc_{1-y}Mg_yO_3$ ($0.05<x<0.08, 0<y<0.02$).

Compounds	Activation energy *E*a (eV)				Conductivity (S/cm) at 1273 K	
	Dry air		Wet H_2		Dry air	Wet H2
	HT	LT	HT	LT		
$Nd_{0.95}Ca_{0.05}ScO_3$	0.80(6)	1.09(14)	0.41(3)	0.69(9)	0.127	0.0056
$Nd_{0.95}Ca_{0.05}Sc_{0.98}Mg_{0.02}O_3$	1.00(7)	1.11(14)	0.61(4)	0.75(10)	0.103	0.0037
$Nd_{0.92}Ca_{0.08}ScO_3$	0.85(6)	0.99(13)	0.48(3)	0.65(9)	0.151	0.0058
$Nd_{0.92}Ca_{0.08}Sc_{0.98}Mg_{0.02}O_3$	1.06(7)	1.18(15)	0.54(4)	0.68(9)	0.186	0.0064

HT: High temprature range (1273–1073 K), LT: Low temprature range (973–673 K).

3.4 Relationship between ionic conductivity and structural parameters

The activation energy and electrical conductivity of the single-phase composition of $Nd_{1-x}Ca_xSc_{1-y}Mg_yO_3$ are listed in Table 1. The activation energies are calculated from the log(σT) vs. 1/T plot, according the following equation.

$$\sigma T = A \exp\left(-E_a/kT\right) \tag{7}$$

where A is constant, E_a is activation energy and k is boltzman constant [21].

Figure 8 shows the relationships between ionic conductivity, the activation energy and *FV* of the unit cell. *FV* was calculated based on the following equations [12, 22]:

$$\text{Free volume } (FV) = V - \text{total volume of the constituent ions}$$

$$V^{1/3} = 2.37r(B) + 2.47 - 2.00(s-1) \tag{8}$$

$$s = \sqrt{2}\frac{r(B)+r(X)}{r(^{XII}A)+r(X)} \tag{9}$$

where $r(A)$ is the effective ionic radius [23] of the A-site cation for ABO_3, r(B) is one of the B-site cations and $r(X)$ is the oxide ionic radius of 1.40 Å.

At 1273 K, it was found that σ was maximized when *FV* was 17.58 $Å^3$, and at 873 K, it was found that σ and activation energy had a linear correlation to *FV*. We believe that the predominant conductive species is oxide ion at 1273 K and proton at 873 K, as shown in Fig. 3. The ionic radius of oxide ion is larger than that of proton. When oxide ion moves in the crystal lattice, considerable activation energy is necessary and mobility is influenced by multiple structural parameters. Therefore, the optimum point of oxide ionic conduction must be identified based on a combination of structural parameters such as *FV*, E_{ab}, r_{crit} and t. It has been reported by Hayashi et. al that the optimum conditions of oxide ion conduction exist due to a balance of structural parameters [12].

On the other hand, the proton conduction mechanism is considered to be a hopping mechanism of protons changing OH- bonds one after another [24]. Nomura et al. discuss the relationship between the oxygen–oxygen distance and the proton conduction pathway [25]. When the O–O bond length of inter-BO_6 octahedra approached those of intra-BO_6 octahedral, it was observed that a change from three dimension to one dimension in the predominant proton conduction pathway in $La_{0.9}Sr_{0.1}M^{III}O_3$ ($M^{III}=Sc^{3+},In^{3+},Lu^{3+}$). This change resulted in a decrease in mobility in proton conduction. Therefore, the proton conductivity in this material is strongly affected by the oxygen–oxygen distance. As shown in Fig. 8, activation energy decreases with increasing *FV*. We believe that a relationship exists between *FV* and the average O–O bond length of inter-BO_6: the longer the O–O bond of inter-BO_6, the larger the *FV* of the unit cell. A long O–O bond will decrease the mobility of proton, and the reverse

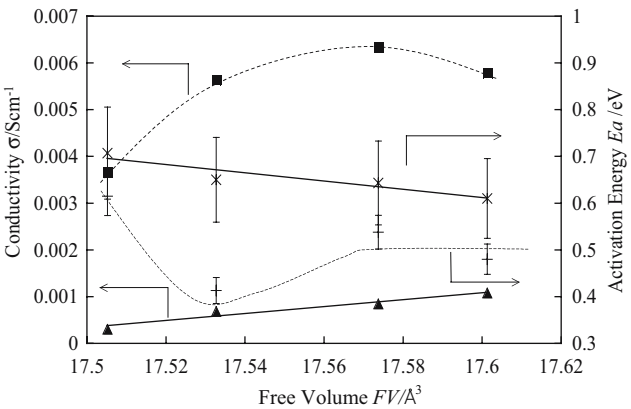

Fig. 8 Relationship between conductivities and free volume (*FV*) for $Nd_{1-x}Ca_xSc_{1-y}Mg_yO_3$ (x=0.05, y=0; x=0.05, y=0.02; x=0.08, y=0; x=0.08, y=0.02). *Filled triangle*: conductivity at 873 K under wet 1% H_2–N_2 balance gas conditions; *Filled square*: conductivity at 1273 K under wet 1% H_2–N_2 balance gas conditions; *Positive symbol*: activation energy in the temperature range from 1273 to 1073 K; *Asterisk*: activation energy in the temperature range from 973 to 673 K

inclination is also shown in Fig. 8. The O–O bond length of inter-BO_6 and the gradient of BO_6- octahedra will also influence the mobility of proton in this series.

4 Conclusion

The electrical conductivities of $Nd_{1-x}Ca_xSc_{1-y}Mg_yO_3$ were measured in the temperature range from 673 to 1273 K under wet and dry conditions and conduction tendencies were examined. We arrived at the following conclusions:

(1) The optimum Ca^{2+} doping concentration to the Nd^{3+} site in $NdScO_3$ is the range from 5 to 10%.
(2) Hole conduction is predominant under dry and highly oxidized conditions of $P(O_2)>10^{-2}$ kPa in the temperature range from 973 to 1273 K; proton conduction is predominant under wet and reduced conditions in the temperature range from 673 to 973 K; and oxide ion conduction is predominant under wet and reduced conditions in the temperature range from 1073 to 1273 K.
(3) The Mg^{2+} doping concentration limit for the Sc^{3+} site to hold a single crystal phase is 2% and this doping was found to enhance hole conduction.
(4) We identified the optimum point for the highest conduction of oxide ions in the series of $Nd_{1-x}Ca_xSc_{1-y}Mg_yO_3$ under reduced conditions in the temperature range from 1273 to 1073 K. Under wet conditions in the temperature range from 973 to 673 K, proton conduction is predominant and we found a linear relationship between conductivity and *FV*.

References

1. S.E. Veyo, in *The 3rd International Fuel Cell Conference: Proceeding*, (NEDO and FCDIC, Japan, 1999), p. 327
2. S.C. Singhal, Solid State Ion. **152–153**, 405 (2002)
3. M. Dokiya, Solid State Ion. **152–153**, 383 (2002)
4. S.E. Veyo, in *Fuel Cell Seminar:Abstracts*, (Palm Springs, CA USA, 1998), p. 457
5. F. Tietz, H.-P. Buchkremer, D. Stover, Solid State Ion. **152–153**, 373 (2002)
6. B.C.H. Steele, Solid State Ion. **129**, 95 (2000)
7. T. Ishihara, H. Matsuda, Y. Takita, J. Am. Chem. Soc. **116**, 3801 (1994)
8. T. Ishihara, H. Matsuda, Y. Takita, Solid State Ion. **79**, 147 (1995)
9. T. Ishihara, H. Matsuda, M.A. bin Bustam, Y. Takita, Solid State Ion. **86–88**, 197 (1996)
10. J.A. Kilner, R.J. Brook, Solid State Ion. **6**, 237 (1982)
11. R.L. Cook, A.F. Sammells, Solid State Ion. **45**, 311 (1991)
12. H. Hayashi, H. Inaba, M. Matsuyama, N.G. Lan, M. Dokiya, H. Tagawa, Solid State Ion. **122**, 1 (1999)
13. K. Nomura, S. Tanase, Solid State Ion. **98**, 229 (1998)
14. D. Lybye, F.W. Poulsen, M. Mogensen, Solid State Ion. **128**, 91 (2000)
15. S. Kim, K.H. Lee, H.M. Lee, Solid State Ion. **144**, 109 (2001)
16. K. Nomura, T. Kakeuchi, S. Tanase, H. Kageyama, K. Tanimoto, Y. Miyazaki, Solid State Ion. **154–155**, 647 (2002)
17. K. Nomura, T. Kakeuchi, S. Kamo, H. Kageyama, Y. Miyazaki, Solid State Ion. **175**, 553 (2004)
18. D. Lybye, N. Bonanos, Solid State Ion. **125**, 339 (1999)
19. H. Fujii, Y. Katayama, T. Shimura, H. Iwahara, J. Electroceram. **2**(2), 119 (1998)
20. H. Kato, T. Kudo, H. Naito, H. Yugami, Solid State Ion. **159**, 217 (2003)
21. J.A. Kilner, Solid State Ion. **129**, 13 (2000)
22. O. Fukunaga, T. Fujita, J. Solid State Chem. **8**, 331 (1973)
23. R.D. Shannon, Acta Crystallogr. **A32**, 751 (1976)
24. H. Iwahara, Solid State Ion. **86–88**, 9 (1996)
25. K. Nomura, T. Takeuchi, H. Kageyama, Y. Miyazaki, Solid State Ion. **162–163**, 99 (2003)